

Themis ESA First Science Results and Performance Issues

J.P. McFadden, C.W. Carlson, D. Larson, and V. Angelopoulos

1. First Results	
1.1 Plasmaspheric Plumes	X
1.2 Conic outflows	X
1.3 Field Line Resonances	X
1.4 Low Latitude Boundary Layer	X
1.5 Magnetopause and FTEs	X
1.6 Bow Shock	X
2.0 Performance Issues	
2.1 Sensor background	
Negligible scattered sunlight photons	X
Photoelectrons	X
Scattered electrons	X
Penetrating radiation	X
2.2 Errors due to Measurement Limitations	
Composition	X
Missing plasma (cold and hot)	X
FOV limitations	X
Affect of E-field on s/c potential, bias sweeps	X
Wrong spin phase when in eclipse	X
2.3 Data Formatting problems	
Mapping errors in ETC early in mission	X
Loss of data at mode transitions	X
Count rate saturation in SS/FS	X
On-board Moment calculation problems	X

1.0 First Science Results from the THEMIS ESA

During the first 9 months of the mission, the THEMIS spacecraft have sampled the dusk, subsolar and dawn regions of the magnetosphere, demonstrating their ability to resolve the basic plasma features of these regions. The THEMIS mission provides the first multi-satellite measurements of the dayside magnetosphere, magnetopause and bow shock with a string of pearls orbit near the ecliptic plane. In this section we will highlight the measurement capabilities of the ESA plasma sensors by presenting observations from several regions in the dayside magnetosphere and upstream solar wind. We do not attempt to provide an in depth science investigation of each of these phenomena, but rather focus on the measurement techniques that allow these structures to be resolved. We begin with structures in the magnetosphere, such as plasmaspheric plumes and field-aligned resonances, and move outward to structures at the magnetopause, magnetosheath, bow shock and foreshock.

1.1 Plasmaspheric Plumes and Cold Plasma

The out-gassing of cold plasma from the ionosphere and the formation of the plasmasphere have long been studied [Carpenter et al. ???Refs]. During active times, magnetospheric convection driven by the solar wind can disconnect the outer portions of the plasmasphere creating plasmaspheric plumes that stretch out to the magnetopause. During magnetic storms the loss of plasmaspheric plasma can be quite large as demonstrated vividly by pictures from the Image satellite [Ref]. In situ measurements of this loss of cold plasma has been recorded by the XX satellites [Ref] and Cluster has observed these cold ions at the magnetopause [Sauvaud et al., ??]. The THEMIS satellites, with their string of pearls orbit, provide dramatic measurements of these plumes. The early orbit configuration has provided a large volume of data on these outflows, demonstrating the increasingly important role that cold plasma appears to play in magnetospheric dynamics.

Figure 1 illustrates a high density cold plasma plume observed by the THC spacecraft near the magnetopause at ~1330 LT (~22 UT) on June 8, 2007. The figure shows electron and ion spectrograms, ion velocity, and density. Spacecraft potential is indicated by the black line on the electron spectrogram. The black line on the ion spectrogram is the proton energy at the drift velocity. Density and velocity calculations include corrections for spacecraft potential, and ion moments are calculated assuming only protons. Cold ions are seen in the second panel when the plasma flow velocity is high enough so that protons penetrate the spacecraft potential. As seen between 2003 UT and 2004 UT, these ions often appear as a monoenergetic beam whose changing energy indicates acceleration of the bulk plasma. Flows this large are often observed near the magnetopause where changes in solar wind pressure cause substantial motion of this boundary and the nearby plasma. When the flow velocity is small, cold plasma can also be indicated by an electron density (red curve) that is much higher than the ion density (black curve) as seen at ~2206 UT in the bottom panel.

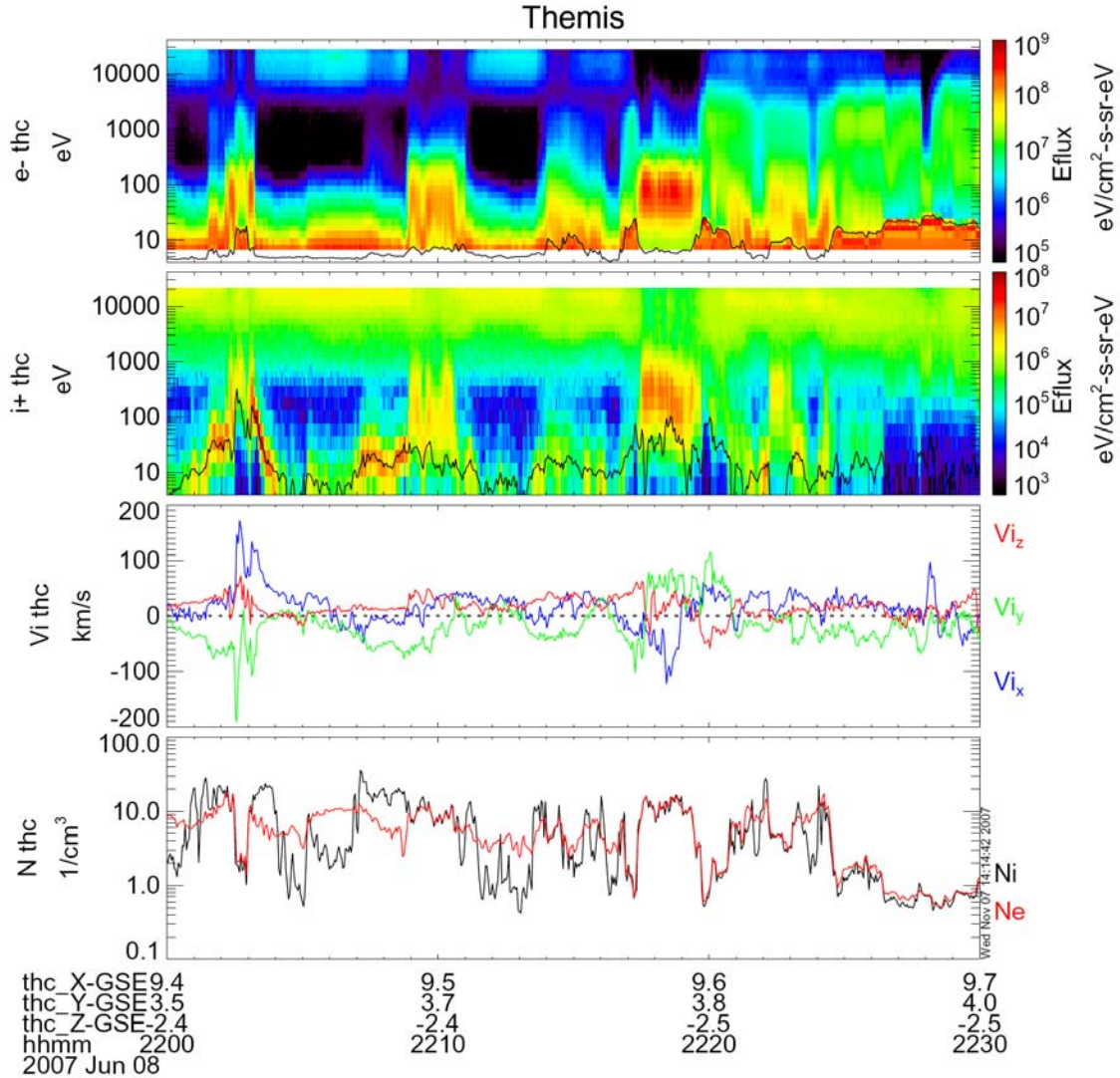


Figure 1: Electron (panel 1) and ion (panel 2) spectrograms, ion velocity (panel 3), and ion (black) and electron (red) densities (panel 4) during a high density cold plasma plume observed by the THC spacecraft near the magnetopause. The black line on panel 1 indicates the spacecraft potential and the black line on panel 2 indicates the energy of protons at the ion flow velocity minus $e\Phi_{sc}$.

An ESA measurement limitation is indicated by this figure. The high density of the plume can drive the spacecraft potential so low that a substantial portion of the electron distribution is not measured. Since the electrons that accompany the plume are also very cold, a substantial underestimate of the electron density can occur as seen at ~2208 UT, when the measured ion density rises above the measured electron density. This discrepancy is not a calibration error since extremely good agreement is obtained between ion and electron densities within the LLBL at ~2210 and 2218 UT, when all the plasma is measured. Such underestimates of cold ion and electron density often occur within the inner magnetosphere. In this case the low spacecraft potential becomes the best indicator of cold plasma. Cross calibrations between measured densities and spacecraft potentials, and a lower limit on ESA sweep energy, may allow a recovery of inner magnetospheric density.

The multi-satellite THEMIS measurements provide global context for plasmaspheric plume studies. The plume in Figure 1 was continuously detected for ~80 minutes in the ESA data on THC. It probably extended back to the plasmasphere since the spacecraft potential remained low throughout this outbound pass until the plume was exited at 22:26:30 UT. All 5 THEMIS spacecraft observed this plume, measuring high-densities ($>10/\text{cm}^3$) and simultaneous magnetopause motions. Similar high-density plumes have been observed on at least 15 orbits, with the highest density plume having $\sim 60/\text{cm}^3$ near the magnetopause. A comprehensive study of these cold plasma measurements is planned for the special issue THEMIS issue of GRL.

1.2 Conic outflows

In addition to the cold ion component described above, whose presence is due to ionospheric outgassing driven by ambipolar fields, a cool ion component is also found in the dayside magnetosphere whose source is ionospheric wave heating. Unlike the cold ions which are only observed with velocities perpendicular to the magnetic field during enhanced convection, the cool ion component consists of field aligned ions that are detected independent of convection. Although the angular resolution of the THEMIS ESA instrument is not adequate to distinguish between ion beams [Ref] and ion conics [Ref], the broad energy of these ions suggests they are conics that have folded up in pitch angle as they moved into regions of lower magnetic field [Ref]. A cursory examination of the dayside data indicates these conics less common than the cold ions, however we expect this to change as the THEMIS spacecraft move into the magnetotail where they can sample auroral ion outflows.

Figure 2 illustrates a conic outflow at ~1340 LT as THD traveled inward from the magnetopause. Conics appear as a broad, low-energy (5-200 eV) band in the ion spectrogram (panel 2). They are observed nearly continuously for more than an hour, decreasing slowly in energy with time. Panel 3 shows that their appearance does not depend on high flow velocities. A more detailed analysis has shown the bulk of their velocity is field-aligned, and sometimes counter-streaming. The top panel demonstrates that the conics are accompanied by a low energy electron component. The bulk of these cool electrons are relatively isotropic however the electrons >100 eV consist of field-aligned counter-streaming electrons.

The bottom panel compares measured electron and ion densities, assuming only protons. The mismatch illustrates a generally problem interpreting THEMIS data when composition is unknown. It is possible that the bulk of ion conics are below the lower energy cutoff of the sensor (~ 15 eV when spacecraft potential is taken into account). However, the conics could also contain significant higher mass ions which would be undercounted in a density calculation that assumed only protons. Other methods must be used to resolve such issues, such as comparisons of the convection velocity between conics and high energy ions. Here we do not attempt to perform this analysis, but instead just remind the user of this limitation of the data.

Lastly, we point out the reconnection flow jets in panel 3 at two of the magnetopause crossing. This event will be examined more fully in section 1.5 below.

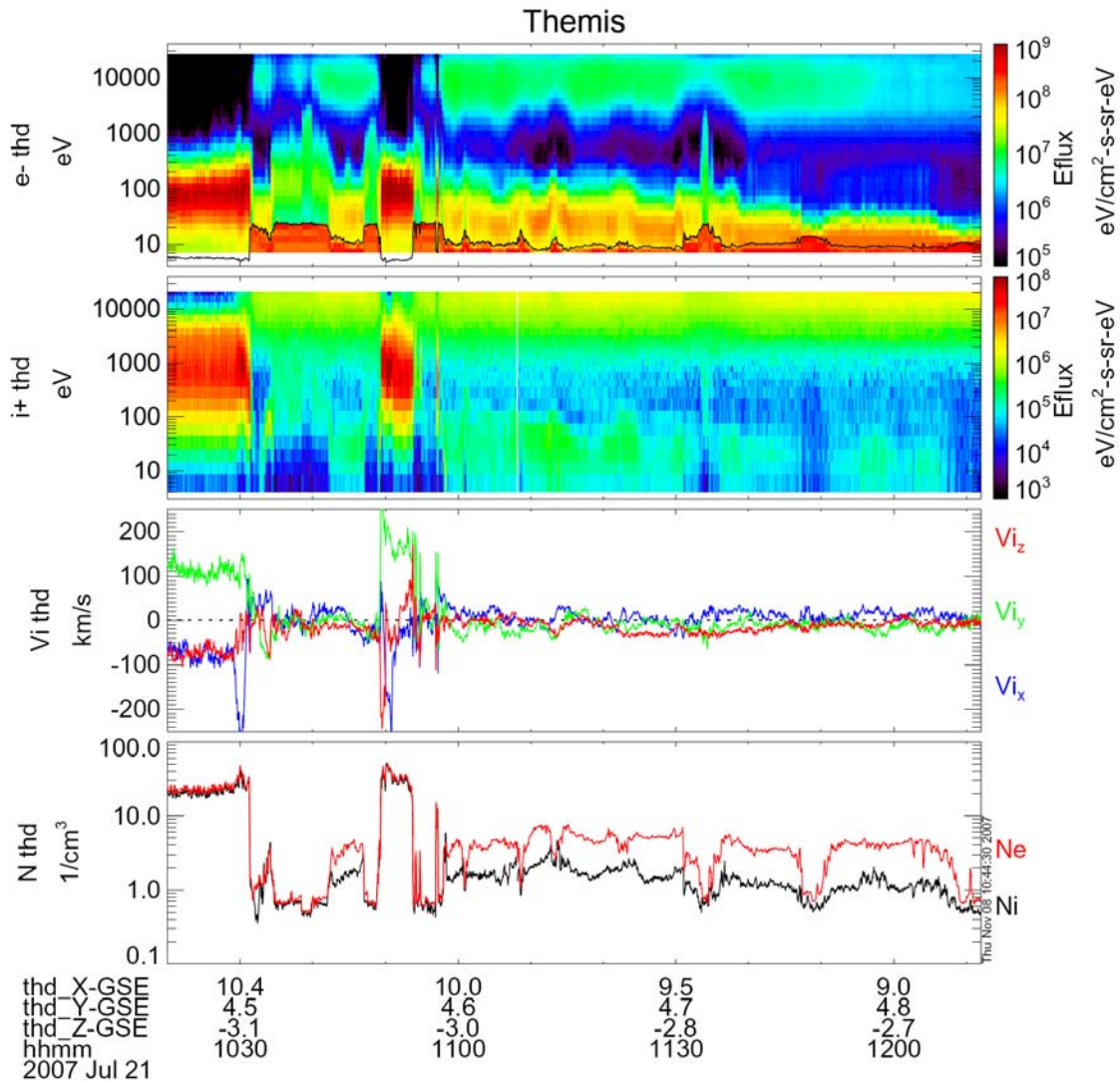


Figure 2: Electron (panel 1) and ion (panel 2) spectrograms, ion velocity (panel 3), and ion (black) and electron (red) densities (panel 4) during a conic outflow at ~1340 LT as THD traveled inward from the magnetopause. Conics appear as a broad, low-energy (5-200 eV) band in the ion spectrogram (panel 2). The mismatch in ion and electron densities could be due to missed cold ions, to conics other than protons, or a combination of both.

1.3 Pc 5 Field Line Resonances

Azimuthally polarized toroidal Pc 5 pulsations are commonly observed by THEMIS in the dusk and dawn magnetosphere. These resonances have a magnetic node at the equator where they exhibit large amplitude plasma motions. There is no agreed upon source but it is thought that modulations at the magnetopause, due to Kelvin Helmholtz instabilities, pressure variations, or changes in reconnection (FTEs), couple energy to these waves

[Refs]. Multi-satellite THEMIS measurements, especially those early in the mission in the dusk sector, can be used to study these FLRs.

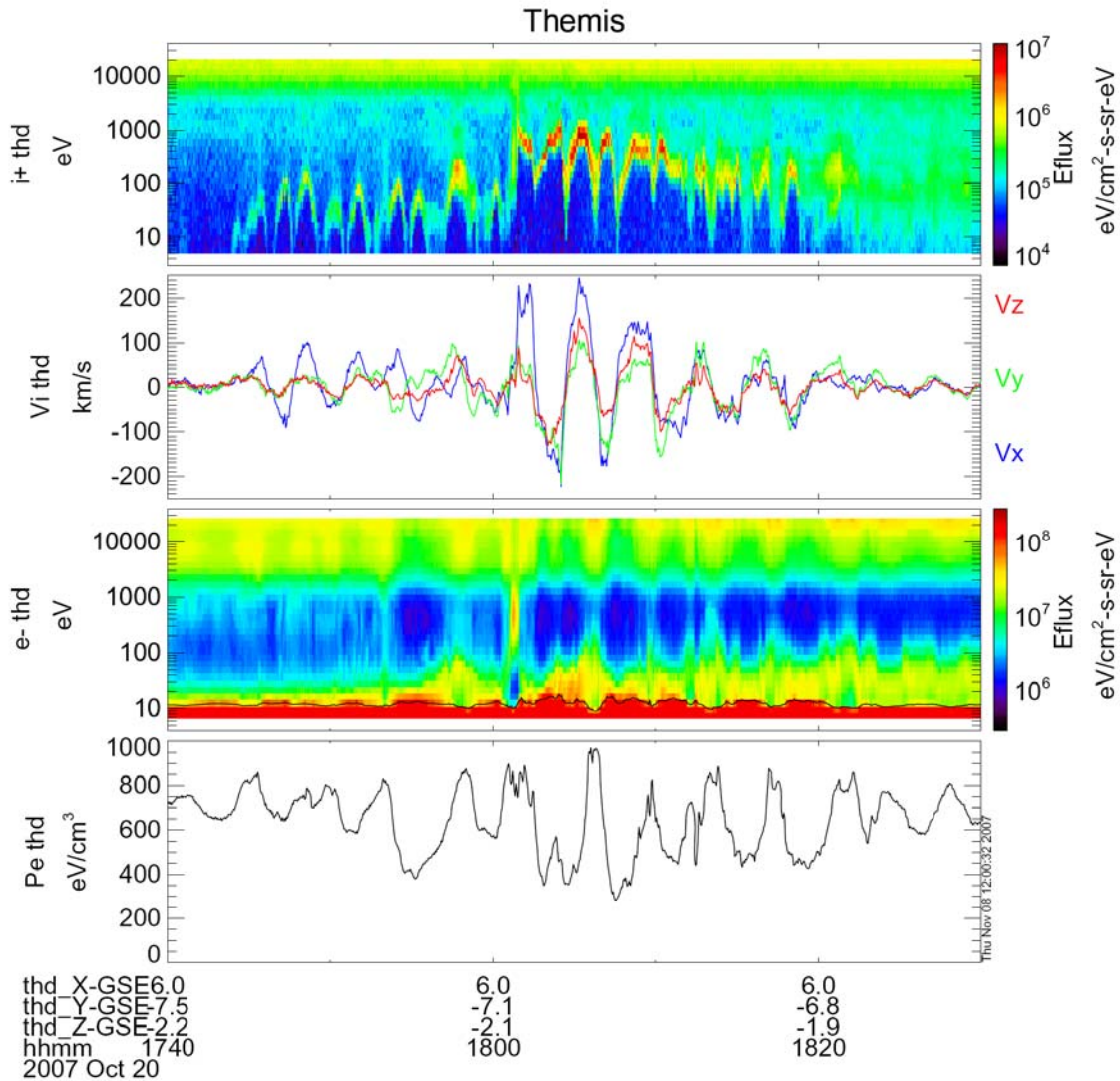


Figure 3: Ion spectrogram (panel 1), ion velocity (panel 2), electron spectrogram (panel 3), and electron total pressure measured by the ESA (panel 4) during a toroidal Pc 5 field line resonance (FLR). Cold ion stand out in the spectrogram, accelerated to keV energies by this wave. Ion velocity is slightly underestimated as explained in the text. Significant modulation of the electron pressure is observed in both the ESA (panel 4) and at higher energies by the SST.

Figure 3 shows an unusually large toroidal Pc 5 event. The resonance motion is easily seen in the ion spectrogram (top panel) where cold plasma ($n_c \sim 1 \text{ cm}^{-3}$) is accelerated to nearly keV energies by the wave. These resonances have been extremely helpful in identifying the cold plasma component near dawn, which often has a density between 0.1 cm^{-3} and 1.0 cm^{-3} . Panel 2 shows the ion velocity determined from the onboard moments (assuming only protons). The dominant amplitude during the wave growth is in GSE x-direction. The subsequent wave decay has nearly equal x and y components, as expected for a toroidal wave at a GSE position of $(6R_e, -7R_e, 2R_e)$. Panel 3 shows that the hot

electron component is strongly modulated by these waves, with nearly order of magnitude pressure variations being observed in the largest events. This pressure modulation may indicate the role that toroidal Pc 5 waves play in electron energization, and in particular a role in the creation of the electron radiation belts. A similar modulation of the ion pressure can also be observed in the ESA data when the temperature is low enough so that the bulk of hot ions are measured.

For future studies of FLRs, there are some measurement problems that limit the accuracy of the calculated plasma moments. The plasma velocity may be underestimated due to a calculation error caused by the energetic electron flux (panel 3). Energetic electrons scattering into the ion sensor produce a small number of counts at low energy that mimic tenuous stationary plasma. These background counts can distort both the density and velocity moments. For example at the peak in flow velocity at 1806 UT, background counts add a false $\sim 0.5 \text{ cm}^{-3}$ to the density estimate. Since cold plasma ($\sim 1.4 \text{ cm}^{-3}$) and hot plasma ($\sim 0.14 \text{ cm}^{-3}$) have about three times this density, the velocity moment is underestimated by $\sim 30\%$ if background is not removed. In addition, the high energy cutoff of the ESA can result in a similar underestimation of the plasma velocity. A better convection velocity estimate can be obtained from the peak in cold plasma spectra. Lastly, since a significant fraction of the plasma pressure can reside above the highest energy step of the ESA, use of SST data may be required for accurate pressure estimates.

1.4 Low Latitude Boundary Layer

The low latitude boundary layer (LLBL) is a complex portion of the magnetopause whose structure changes dramatically with local time and with orientation of the magnetosheath IMF. The LLBL can change from a thick layer with a substantial plasma depletion layer (PDL) during northward IMF, to a thin layer with reconnection jets and flux transfer events (as described in section 1.5). In this section we provide an example of THEMIS data during northward IMF when dual-lobe reconnection traps magnetosheath plasma onto closed field lines forming a thick LLBL.

Figure 4 shows a subsolar crossing of the LLBL during northward IMF as the THC travels from the magnetosheath to magnetosphere. The PDL is observed from 850 UT to ~ 906 UT and is characterized by an increase in magnetic field (panel 1), a significant decrease in density (panel 2), and a small drop in velocity (panel 3). The transition from PDL to LLBL is indicated by the tenuous energetic tail in the electrons (panel 5) starting sporadically at ~ 905 UT. These electrons are the first indication of lobe reconnection in one or both hemispheres [Ref]. THC travels through the LLBL and enters the magnetosphere at ~ 913 UT as seen by the presence of hot ions (panel 4) and hot electrons (panel 5). Magnetopause motion causes THC to re-enter the LLBL at ~ 916 UT before finally crossing back into the magnetosphere at ~ 928 UT. These and other multi-satellite measurements with 3 s resolution of the plasma distribution should allow THEMIS to completely characterize the LLBL during its mission.

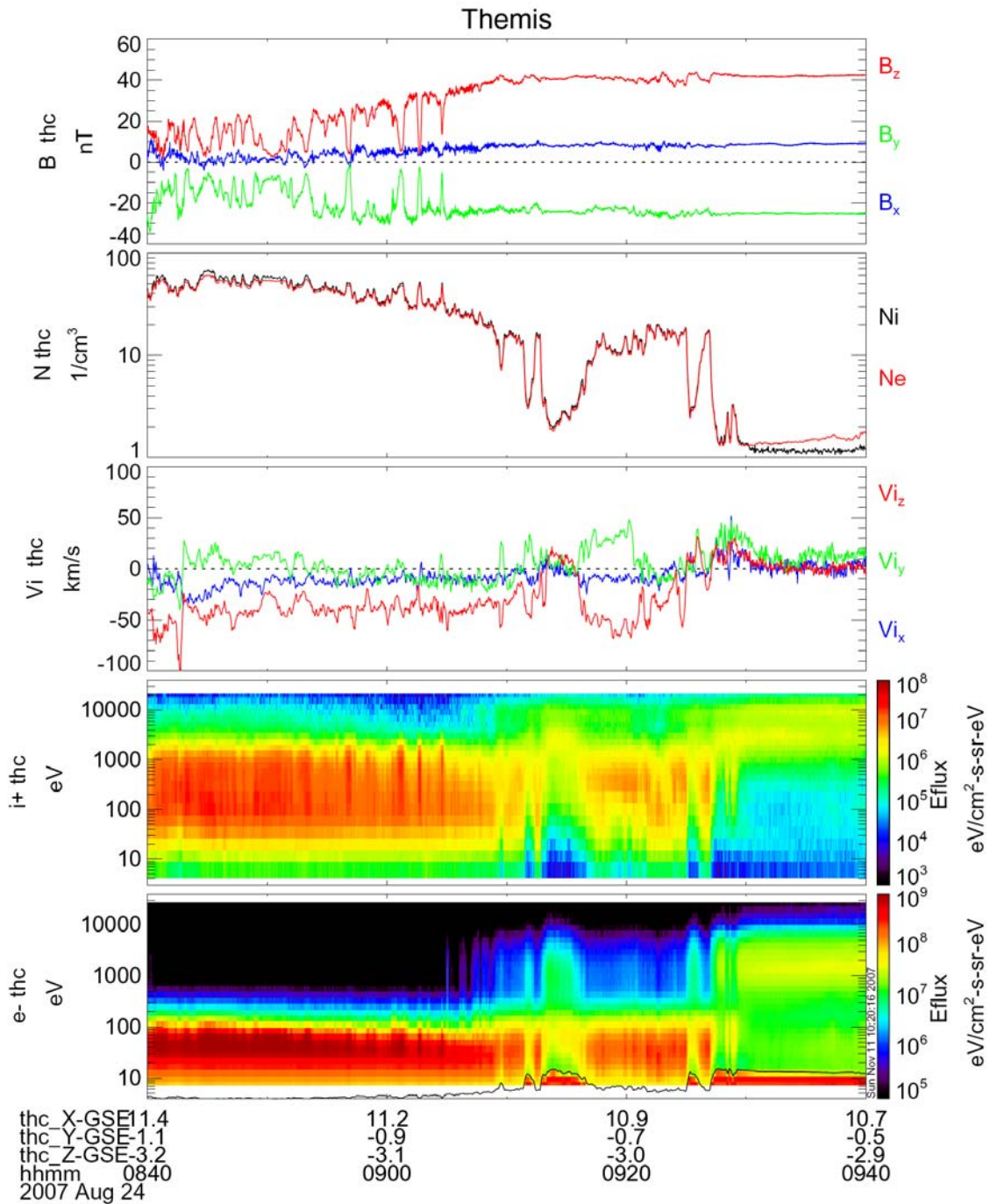


Figure 4: Magnetic field (panel 1), ion (black) and electron (red) densities (panel 2), ion velocity (panel 3), and ion (panel 4) and electron (panel 5) spectrograms during a LLBL crossing near the subsolar point. A plasma depletion layer (PDL) present from 8:50 to 9:05 as indicated by the decrease in density and increase in magnetic field. The transition to lobe-reconnected field lines is indicated by electrons >1 keV.

1.5 Magnetopause and FTEs

Flux Transfer Events (FTEs) are a common feature of the dayside magnetopause. They are believed to result from multiple reconnection lines forming plasmoids or flux ropes in

a manner similar to plasmoid formation in the magnetotail. FTE signatures were initially observed in magnetometer data [Russell and Elphic, ??] with a variety of signatures [Elphic et al., 19??]. The plasma signatures of FTEs were observed later [Refs] and current 3-D simulations are now manifesting similar structures.

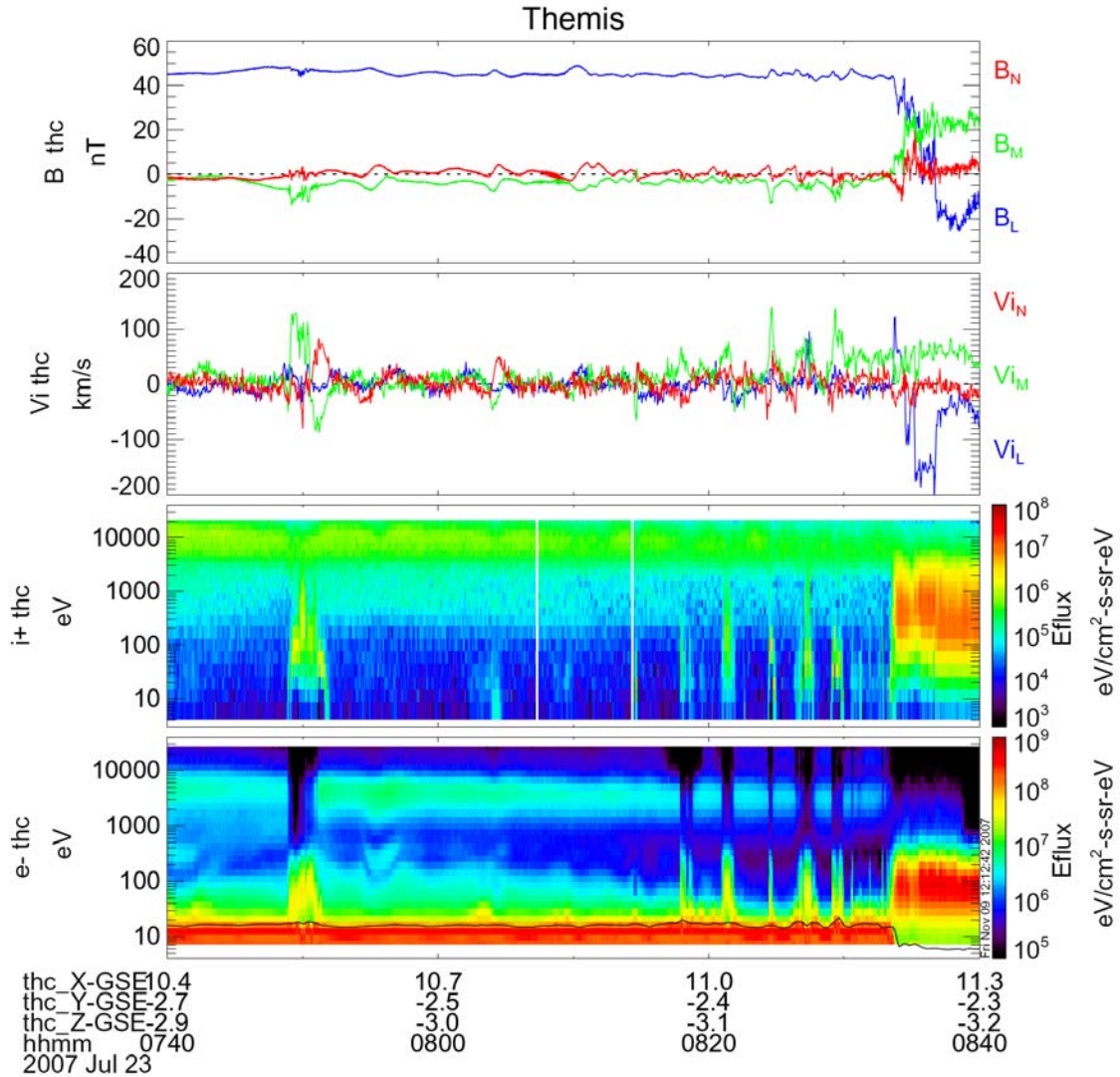


Figure 5: Magnetic field (panel 1), ion velocity (panel 2), and ion (panel 3) and electron (panel 4) spectrograms during a magnetopause crossing with flux transfer events (FTEs). The motion caused by the passage of the FTEs reveals cold plasma which can become trapped in the FTEs. The large ion flow at the magnetopause is suggestive of a reconnection jet.

Figure 5 illustrates a THEMIS magnetopause crossing during southward IMF which contains at least nine FTEs. FTEs can be identified in both the magnetic field and in the plasma velocity, both of which have been rotated to LMN coordinates. Cold plasma adjacent to the magnetopause can be identified in the ion spectrogram (panel 3) either when plasma motion occurs adjacent to the FTE or when the FTE traps this cold component. The electron spectrogram in the bottom panel allows easy identification of field lines which have reconnected and lost their hot magnetospheric electrons. These hot electrons are replaced by a cooler magnetosheath population which often have

counterstreaming distributions. In addition, a reconnection jet can be seen as the magnetopause is crossed at $\sim 8:37$ UT. THEMIS's multi-satellite measurements of FTEs, including detailed plasma measurements at spin period resolution, should provide an invaluable dataset on the structure of the magnetopause.

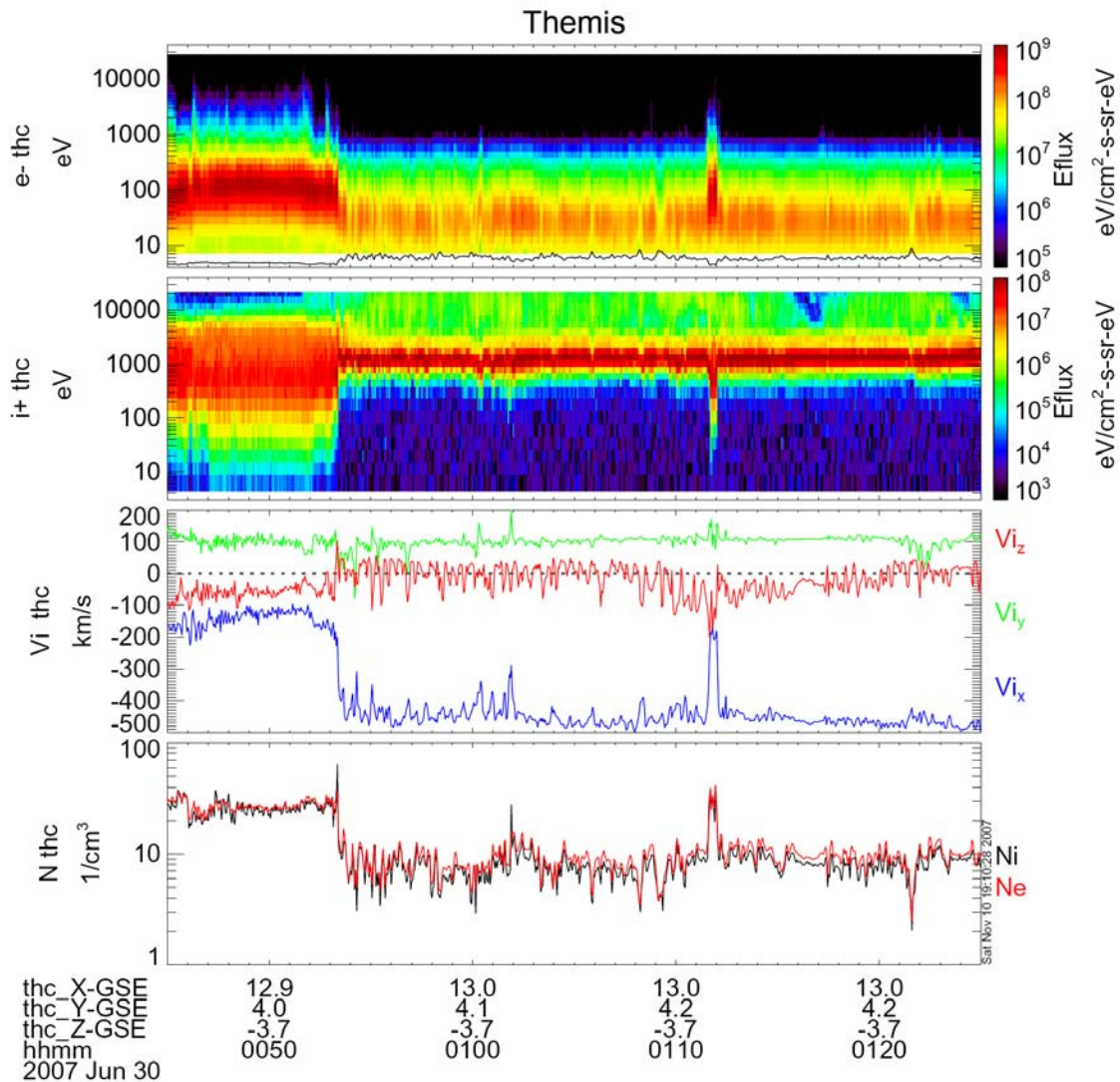


Figure 6: Electron (panel 1) and ion (panel 2) spectrograms, ion velocity (panel 3), and ion (black) and electron (red) densities (panel 4) near a quasi-parallel bow shock. 30 s waves (panel 3) dominate the turbulent upstream region, along with energetic gyrating ions (panel 1).

1.6 Bow Shock

The structure of the bow shock has been observed and cataloged by numerous satellite missions. These measurements have revealed a complex structure whose dynamics is primarily controlled by the orientation and magnitude of the IMF. Shock structure includes gyrating ions upstream of the quasi-perpendicular shock, the wave-like structure and reformation of the quasi-parallel shock, upstream foreshock particles that

precondition the solar wind, SLAMS, Hot Flow Anomalies (HFAs), 30 s period modulations of the upstream IMF, and solitary structures. All of these structures have been observed by THEMIS during the first nine months of operations. Although the sensor was not optimized for the solar wind, it performs quite well under nominal conditions. The primary error will result from high density cold flows which can saturate the ion sensor, or high densities which can saturate the electron counters (especially in slow survey mode where an omni-direction spectra are taken). The unique THEMIS orbits that skim along the subsolar bow shock should provide data that will allow continued progress on shock physics.

Figure 6 shows an example of THEMIS observations near the quasi-parallel bow shock. On this orbit, the spacecraft spent significant time in the upstream region sampling plasma in the 30 s waves upstream of the shock. When the spacecraft are operated in fast survey (as in the figure), the magnetospheric mode records 3-D ion distributions at spin resolution which allow accurate ion moments computed on the ground, as confirmed by the density comparison in the bottom panel. Onboard moments are also available starting in August of 2007.

2.0 Performance Issues

Before embarking on analysis of the THEMIS ESA data, it is important for the scientist to be aware of various performance issues with ESA data: sources of background, non-ideal response of the instrument, limitations due to missing information, and telemetry formatting problems. The data set is too large for the subset of problem data to be routinely corrected or purged from the files. Instead the scientist should be aware of these data limitations in order to avoid periods where non-geophysical interference or missing information can result in misinterpretation of the observations. In this section we outline known performance issues associated with the THEMIS ESA data that were uncovered during the first nine months of operations.

2.1 Sources of sensor background counts

When performing detailed analysis of data from the THEMIS ESAs, care should be taken to assure that non-geophysical sources of counts do not affect the result. There are several sources for this background: 1) Solar UV scattered directly into the detector, 2) photoelectrons produced by solar UV that reach the detector, 3) energetic electrons scattered through the sensor to the detector, and 4) penetrating radiation.

2.1.1 Scattered UV

As of this paper, there is no indication of measurable counts due to solar UV scattered to the detectors. However, the THEMIS spacecraft have yet to sample the magnetotail lobes where plasma count rates are generally the lowest, allowing more sensitive measurements of this background. This region will be sampled in the winter of 2008 and offers the best possibility of quantifying scattered solar UV. Based on previous instruments, such as Cluster-HIA, we expect peak count rates of $\sim 50/s$ limited to a narrow angle range ($\sim 13^\circ$) when the sensor faces the sun (see Carlson and McFadden, 1998).

2.1.2 Photoelectrons

Spacecraft photoelectrons are a source of non-geophysical counts in the electron ESA. This photoelectron contamination comes from three different sources: Langmuir probes, spacecraft surfaces, and internal sensor surfaces. This contamination can often be removed from the measurement when the spacecraft potential is known. Photoelectrons with energy greater than the spacecraft potential generally escape into the plasma, therefore the spacecraft potential provides a relatively clean separation, or cutoff energy, between reflecting photoelectrons and the in situ plasma. However, there are photoelectrons that appear at energies above the spacecraft potential that may require consideration if precise measurements are required.

The most prominent photoelectron contamination comes from the Langmuir probes as illustrated in Figure 7a. Since these probes float near the local plasma potential, they produce photoelectrons shifted in energy by nearly $e\Phi_{sc}$. These photoelectrons dominate over spacecraft photoelectrons near the cutoff energy, $e\Phi_{sc}$, and can generally be

eliminated from moment calculations since they are confined to only one or two energy bins. However, when a cold population of electrons is present in the plasma, as often happens in the inner magnetosphere, it may be difficult to cleanly separate the photoelectrons from the plasma. Current observations suggest most cold plasma electrons are warmer than the photoelectron population, so modeling this population may provide a reasonable separation in a moment computation.

In addition to the Langmuir probe photoelectrons, the EFI instrument has several other antenna surfaces (usher, guard and braid) that can be voltage biased relative to the probes. On THC from May 26 to June 22, 2007, the usher and guard were biased 8 V negative relative to the Langmuir probes producing photoelectrons ~ 8 eV above the probe potential. These are illustrated in Figure 7b where the axial antenna introduces photoelectrons at ~ 10 eV into the polar angle bins of the ESA. Similar electrons from the radial probes are not apparent. Prior to May 26 the usher was 6 V positive, but the guard was 20 V negative relative to the probe, resulting in ~ 19 eV electrons above spacecraft potential. Although most of these electrons escaped to space, some are observed in the electron sensor, especially in the polar bins that look along the spacecraft surface and record photoelectrons from the axial probes. After June 22, 2007, photoelectrons from the usher, guard, and braid generally appear at energies below the spacecraft potential. Similar photoelectrons were observed on THD and THE after their boom deployments (June 2-6, 2007) until the bias changes on June 22, 2007.

Starting July 20, 2007 the braid was driven at the same voltage as Langmuir probe 1 (on THC, THD, THE) to improve the EFI response. Starting about October 29, 2007 on THD and THE, and November 6 on THC, the spacecraft entered portions of the orbit where the spacecraft body shadowed the Langmuir probes each spin for ~ 25 ms. This resulted in the voltage on the shadowed probe charging to -85 V relative to the spacecraft, the upper limit of the EFI power supplies. Since the braid on all four antenna were tied to probe 1, the sunlit braids on antennae 2, 3 and 4 would produce a ~ 25 ms burst of photoelectrons that could be seen in the electron ESA as illustrated in Figure 7c between 15 eV and 60 eV. The antenna shadowing ended by November 9, 2007 on THD and THE. By November 16, the braid on THC was switch back to ground to prevent further contamination. The current plans are to change EFI operating modes during shadowing periods to prevent this contamination in the future.

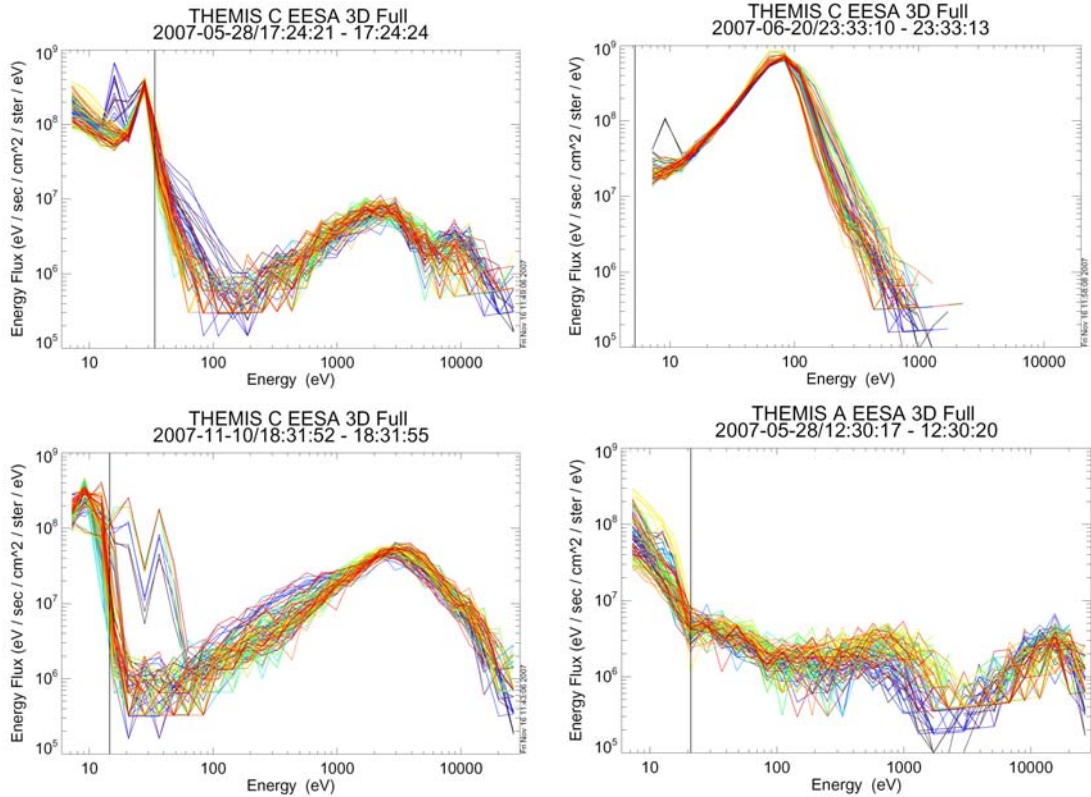


Figure 7: Electron spectra showing: a) photoelectrons from the axial (15 eV) and radial (28 eV) Langmuir probes, b) a photoelectron peak (10 eV) above the spacecraft potential caused by the axial Langmuir probe usher and guard being biased -8 V relative to the probe, c) photoelectrons (15-60 eV) produced in a 25 ms burst when EFI probe shadowing resulted in the EFI braids charging to -85 V relative to the spacecraft, and d) spacecraft photoelectrons at energies below the spacecraft potential measured prior to EFI boom deployment. The spacecraft potential relative to the plasma is indicated by vertical lines.

Spacecraft photoelectrons are the second most prominent contamination to the electron sensor. An electron spectra taken prior to EFI boom deployment is shown in Figure 7d, with photoelectrons appearing below the spacecraft potential indicated by the vertical line. Without EFI's measurement of Φ_{sc} , eliminating these photoelectrons from moment calculations is often difficult, with no clear spectral break to allow determination of Φ_{sc} . However, since photoelectrons are expected to have relatively constant spectra, Φ_{sc} could be estimated from the deviation between a measured low energy spectra and a characteristic photoelectron spectra.

Internally produced photoelectrons in the sensor aperture constitute a third form of photoelectron background. These electrons are produced over about 20° of spacecraft rotation centered on the sunward direction and generally enhance only the lowest energy (<10 eV) bins. These electrons do not generally introduce errors to moment calculations unless the spacecraft potential is small, and small potentials occur during high densities which minimized their impact on moments. Since they are confined to low energies and a few angular bins that look toward the sun, they can be easily removed from a distribution if needed for precise moment calculations.

2.1.3 Scattered Electrons

A third source of background electron ESA counts results from scattered energetic electrons. The impact of these scattered electrons is difficult to estimate for most geophysical distributions. This is because magnetospheric electrons generally have rather broad energy spectra that are either roughly Maxwellian or a superposition of Maxwellians. Therefore, scattering merely results in a slight broadening of the angular and energy distributions. Since the cross-calibrations include this scattering, it generally has no impact on density calculations and only a slight impact the temperature. The one caveat to this behavior is associated with highly peaked electron distributions as found in auroral acceleration regions. Energetic electron beams can produce significant counts at the lowest energies, and therefore may produce an error in the density.

Scattered electrons are also observed in the ion ESA. The primary difference between electron and ion sensor sensitivity to this scattering results from the -2 kV potential at the front of the ion detector. This potential forces scattered electrons to be greater than a few keV before they are observed in the sensors. Electrons at these energies are often present within the magnetosphere and can result in significant errors in the ion density moments since ion count rates are generally much lower than electron count rates. Care must be taken when calculating ion density moments to determine the impact of this contamination.

Figure 8: scattered e- contamination????

2.1.4 Penetrating Radiation

A fourth source of background results from penetrating radiation found in the inner magnetosphere. This background produces flat spectra, with increasing count rate as the spacecraft approaches perigee. Figure 8 illustrates the impact of this background on energy-time spectrograms and density moments for electrons and ions. Background subtractions that reduce this contamination have been developed for the FAST mission [K. Seki, private communication], and could be applied to THEMIS if required for science analysis.

Figure 9: spectrogram with penetrating radiation and scattering????

2.2 Errors due to Measurement Limitations

In this section, we remind the reader of the primary measurement limitations that can prevent precise calculation of plasma distributions and moments of the distributions. We begin with the limitations to the ESA plasma measurement, describing the primary missing components and their impact on moment calculations. Measurement limitations are also associated with invalid information from other instruments, and we elaborate on problems with EFI potential measurements and spacecraft attitude.

Although in most regions of the magnetosphere the THEMIS ESA plasma instruments provide an accurate measurement of the bulk of the plasma, this instrument does not

measure all of the plasma, nor does it measure all the properties of the plasma. Significant errors can occur due to composition changes. Software developed for ESA data analysis assumes the measured ions are protons. In a density calculation, a higher mass ion's contribution to density will be incorrectly underestimated by the factor $(m/q)^{1/2}$. For example, in the magnetosheath an alpha to proton ratio of 10% can produce a ~11% difference in the ion to electron density ratio. Mass density estimates can be skewed even more than number density, especially if significant oxygen is present. Composition can also affect the velocity moment, with higher mass ions recorded as having higher velocity by the ratio of $(m/q)^{1/2}$, and therefore introducing an error similar to the density error. Pressure is generally less affected by composition since pressure is proportional to particle energy and the sensor measures E/q . However if there are large flows, errors in the velocity calculation can impact the dynamic pressure, and therefore affect the pressure tensor which is given by the momentum tensor minus the dynamic pressure. (check this)

Another source of error in plasma measurements is due to missing plasma. Since spacecraft generally charge positive to attract photoelectrons (when in sunlight and when the density is less than $\sim 300/\text{cm}^3$), cold ions are often missed. As discussed in section 1.1, the cold ions often dominate the density within the dayside magnetosphere. Although their presence greatly impacts ion density measurements, higher order moments are generally not affected by their presence. However, the ion plasma sensor's upper energy limit of ~ 25 keV may impact higher order moments, especially within the inner magnetosphere where the ion temperatures are high, or within the plasmashet where high flow velocities can result in missed ions. We suggest that the ion SST ion data be checked, or combined with the ESA data, when high velocities or pressure variations are important to the physics. Lastly we point out that missing plasma in the electron sensor, although less of a problem, may still be significant. A cold ion component is often accompanied by a cold electron component which can be difficult to separate from spacecraft photoelectrons (see section 2.1.2), and on occasion, especially in the inner magnetosphere, hot electron can be significant.

Figure 10: Should we include an example where SST pressure is significant?

Two other measurement limitations in the ESA sensor are related to its field-of-view. Since the sensor only looks in a half-plane at any instant, time aliasing during a spin can skew the measurement. This is especially true for electron velocity moment calculations. Few percent density variations during a spin can result in large (~ 100 km/s) errors in the calculated flows, depending upon electron temperature. These errors are primarily confined to the spin plane since the sensor continuously measures in both directions along the spin axis.

Figure 11: Comparison of electron and ion velocities to show affect of density fluctuations.

The second measurement limitation is the $\sim 6^\circ$ FWHM sensor field-of-view in the half-plane. Since nominal energy sweeps occur during $\sim 11^\circ$ of rotation, narrow beams might be missed. Examples of such narrow beams would include anti-earthward accelerated auroral electron beams and the solar wind ion beam. The ESA instrument has a solar

wind mode with 64 sweeps/spin (5.6° resolution), that can resolve the solar wind ions, however it is not always used in the solar wind. In addition, the high ion count rates in the solar wind can result in significant dead time corrections to these data introducing additional errors.

Since knowledge of spacecraft potential is essential for correct transformations of measured counts to plasma distribution function, EFI measurements are required. Start dates where valid EFI potential measurements are initially available are listed in Table 1. Prior to EFI deployments, spacecraft potential will have to be estimated from the plasma measurements alone. Even after EFI sensor deployment, there are periods where the EFI data may be less than ideal. The EFI Langmuir probes are designed for sunlit conditions, therefore when the spacecraft are in eclipse the probe potential does not provide a good estimate of spacecraft-to-plasma potential. During sensor diagnostic sweeps, which are occasionally run and can take several hours, spacecraft potential measurements can be invalid. The bias currents to the Langmuir probes, and the associated voltages on adjacent surfaces, have been changed several times during the first year resulting in different functional relationships between spacecraft-to-probe potential and spacecraft-to-plasma potential. Lastly, during periods with restricted telemetry rates, EFI data may not be at the same cadence as the plasma data, resulting in time aliasing problems at steep density gradients. Since there are several sources of spacecraft-to-probe potential measurements and since these sources have variable time resolution, care must be taken to select the appropriate data type as an input to the plasma data calculations.

Table 1: EFI boom deployment dates

One additional source of error in the plasma measurements can occur during eclipse when sun-sensor data is unavailable to organize spin-synchronous plasma data. As sun pulses disappear, the IDPU will shift into a “fly-wheel mode” that assumes the spin rate is constant. However, small changes in spin period due to thermal contraction of the booms and fuel result in a drift in the orientation at the start of a spin. Although this drift is small, the accumulated error can be significant by the time the spacecraft exits the Earth’s shadow. The primary error is therefore in the orientation of vector and tensor quantities such as the plasma velocity and pressure tensor. Errors to scalar quantities such as density and temperature are negligible. In principle these orientation errors could be corrected with modeling, but at the time of this publication there are no plans to develop this code.

2.3 Errors due to Data Formatting Problems

At the start of the THEMIS mission, several data formatting problems in the ETC board were discovered. The ETC contains mapping tables that are loaded from a PROM at the start of a mode. For ESA 3-D data products (survey, burst and reduced data products), energy maps and an angle maps are used to direct and sum the counter readouts into data product arrays. It was discovered that an occasional bit error would occur in the table load if the processor was simultaneously performing other tasks at the time. These bit errors generally caused some elements of the product arrays to be zero and resulted in

other data products receiving these counts. These bit errors were generally confined to only a few of the 30 3-D data products generated by the 5 satellites, with the subset of tainted products changing with each mode change. The misdirection of data was discovered early during the ESA commissioning phase, and software changes to eliminate processor conflicts during table loads were implemented on all spacecraft by April 27, 2007. Prior to this date, care should be taken in interpreting ESA data, especially any moment computations.

A second data formatting error occurs at the transition between instrument modes. Instrument mode transitions are associated with both configuration changes, such as transitions from magnetospheric mode to solar wind mode, and operational changes, such as transitions from Fast Survey to Slow Survey. In both cases, the transition between table maps and data packet formatting result in the loss of data. Depending upon the data product, and in particular the number of spin-snapshots in a data packet, these transitions result in a data loss or incorrectly formatted data for a few seconds to a few minutes.

A third data formatting problem results from ETC counter saturation and is confined to reduced data products. During slow survey mode, reduced data packets are formed by averaging all counts over a spin into a single energy spectrum. High count rate data, such as electron data in the magnetosheath, often result in counter saturation at the peak in the spectrum. The ETC is designed not to overflow and saturation is easily recognized in the data. During the most intense magnetosheath events, saturations may also be observed in the ion, slow-survey, reduced data products, and in the electron, fast-survey, reduced data products.

Early in the mission, data formatting problems also plagued the onboard moment computations performed by the ETC. In particular the same table load bit errors seen in the 3-D products were present in the moment calculations. Since the moment tables are several orders of magnitude larger than the 3-D data product tables, detection and correction of errors is nearly impossible. In addition, an error in the PROM resulted in the loss of one of the components of the velocity moment (V_y), and incorrect ordering of higher moment components in the moment data packet. Although some onboard moment data can be extracted from these early data, we strongly recommend working with THEMIS team members before incorporating these data in science papers. Corrections to the flight software were not implemented until August 6, 2007, and additional problems we spacecraft potential corrections were present between November 18 and 22, 2007. Lastly, we point out that electron moments are generally invalid on THA and THB until after the boom deployments (November 18, 2007 for THB and mid-January, 2008 for THA) due to lack of spacecraft potential corrections.

References

Bonnell et al.,

Ogilvie, K. W., D. J. Chorney, R. J. Fitzenreiter, F. Hunsaker, J. Keller, J. Lobell, G. Miller, J. D. Scudder, E. C. Sittler Jr., R. B. Torbert, D. Bodet, G. Needell, A. J. Lazarus, J. T. Steinberg, J. H. Tappan, A. Mavretic, and E. Gergin, **SWE, a comprehensive plasma instrument for the WIND spacecraft**, *Space Sci. Rev.*, 71, 55-77, 1995.

Goruganthu, R. R., and W. G. Wilson, Relative electron detection efficiency of microchannel plates from 0-3 keV, *Rev. Sci. Instrum.* 55(12), 2030, 1984.

Gao, R. S., P. S. Gibner, J. H. Newman, K. A. Smith, and R. F. Stebbings, Absolute and angular efficiencies of a microchannel-plate position-sensitive detector, *Rev. Sci. Instrum.*, 55(11), 1756, 1984.

Straub, H. C., M. A. Mangan, B. G. Lindsay, K. A. Smith, and R. F. Stebbings, Absolute detection efficiency of a microchannel plate detector for kilo-electron volt energy ions, *Rev. Sci. Instrum.*, 70(11), 4238, 1999.

Figure Captions

Figure 1 illustrates a high density cold plasma plume

Figure 2 illustrates a conic outflow at ~1340 LT as THD traveled inward from the magnetopause.

Figure 3 shows an unusually large toroidal Pc 5 event.

Figure 4 shows a subsolar crossing of the LLBL during northward IMF as the THC travels from the magnetosheath to magnetosphere.

Figure 5 illustrates a THEMIS magnetopause crossing during southward IMF which contains at least nine FTEs.

Figure 6 shows an example of THEMIS observations near the quasi-parallel bow shock.

Figure 7 An electron spectra taken prior to EFI boom deployment is shown with photoelectrons indicated.

Figure 8. Internally produced photoelectrons in the sensor constitute a third form of photoelectron background. These electrons are produced over about 20° of spacecraft rotation centered on the sunward direction

Figure 9 illustrates the impact of this background on energy-time spectrograms and density moments for electrons and ions.